Chemical Engineering Journal 287 (2016) 492–502

Contents lists available at ScienceDirect

Chemical Engineering Journal

journal homepage: www.elsevier.com/locate/cej

Validated modeling of bubble growth, impingement and retraction to predict cell-opening in thermoplastic foaming

D. Tammaro [a], G. D'Avino [a], E. Di Maio [a,*], R. Pasquino [a], M.M. Villone [b], D. Gonzales [c], M. Groombridge [c], N. Grizzuti [a], P.L. Maffettone [a]

[a] Dipartimento di Ingegneria Chimica, dei Materiali e della Produzione Industriale, University of Naples Federico II, P.le Tecchio 80, I-80125 Napoli, Italy
[b] Center for Advanced Biomaterials for Health Care @CRIB, Istituto Italiano di Tecnologia, Largo Barsanti e Matteucci 53, 80125 Napoli, Italy
[c] The Procter and Gamble Company, Newcastle Innovation Centre, Whitley Road, Longbenton, NE12 9TS, United Kingdom

HIGHLIGHTS

- The sequence of operations involved in gas foaming process is modeled.
- The dynamics of bubble growth and impingement is used to predict rupture and retraction.
- A new retraction criterion is proposed for bubble wall opening.
- The model is validated with poly(ε-caprolactone) foamed with CO_2.

GRAPHICAL ABSTRACT

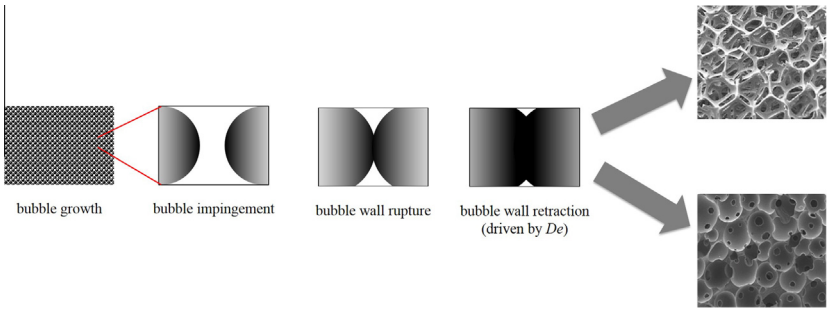

ARTICLE INFO

Article history:
Received 20 July 2015
Received in revised form 5 October 2015
Accepted 6 November 2015
Available online 17 November 2015

Keywords:
Foaming
Open-cell
Modeling
Elastic recovery

ABSTRACT

In this work a design tool to control cell-opening in gas foaming of thermoplastic polymers is developed. The sequence of events following bubble nucleation, namely, bubble growth and impingement, is modeled to gain a comprehensive, perspective view on the mechanisms of bubble wall rupture and on the conditions for achieving a fully open-cell morphology. In particular, unlike the previously published literature, the polymer elastic recovery is recognized as an important factor for wall retraction, which is typically considered as solely driven by surface tension. The new approach is experimentally validated on poly(ε-caprolactone) (PCL), foamed with CO_2, as a model polymer/gas system.

1. Introduction

Due to their mass and energy transport, acoustic absorption, catalytic, impact, and cushioning properties, open-cell polymeric foams are used in a multitude of different applications, including transportation, construction, packaging, food, extraction and separation [1], as well as in leisure and sport. They are also used in tissue engineering, as culture substrates for living cells [2], and as templating structures for ceramic and metal foams.

The *gas foaming technology*, which makes use of a physical blowing agent (e.g., carbon dioxide or nitrogen) to form bubbles in a softened polymer, is the most used process for the making of open-cell foams, mainly because of its high productivity. The sequence of operations involved in the gas foaming technology, specifically for the case of open-cell foams, is: (i) blowing gas solubilization at high pressure (to achieve a polymer/gas solution); (ii) bubble nucleation induced by an instantaneous pressure quench; (iii) bubble growth; (iv) bubble impingement (where the growing bubbles start

* Corresponding author. Tel.: +39 081 768 25 11; fax: +39 081 768 24 04.
E-mail address: edimaio@unina.it (E. Di Maio).

http://dx.doi.org/10.1016/j.cej.2015.11.034
1385-8947/

"feeling" each other, and the polymeric layer separating them progressively thins); and (v) bubble wall rupture [1].

In the last decades, a large number of scientific papers has dealt with the modeling of the above steps, both in order to understand the underlying physico-chemical phenomena and to optimize process conditions. Today, step (i) is quite well understood, in particular how to form the polymer/gas solutions and how much the presence of the solubilized gas affects the thermal [3], mass transfer [4], sorption [5], rheological [6–10], interfacial and volumetric properties [11] of the polymer. More recently, the specific interactions occurring between the polymer and the gas molecules have been considered, opening the way to the design of novel blowing agents [12,13].

Moving to step (ii) above, gas supersaturation is induced by imposing a rapid pressure drop on the polymer/gas solution. The subsequent bubble nucleation is typically modeled by the classical nucleation theory, where the original formulation, developed for water vapor droplets, is adapted to foaming to take into account gas solubility and the high molecular weight of the expanding material [14–16].

Bubble growth (step (iii)) is modeled by mass and momentum (and, in a few cases, also energy) balance equations. Recently, taking advantage of the improved calculating tools, the standard, purely viscous constitutive equations have been substituted by more realistic equations for viscoelastic fluids [17–20].

In some cases, in order to gain some predictive capability on the final foam structure, the nucleation and growth steps are coupled by the so-called *influence volume* approach [21], which assumes that, in the volume of the polymer/gas solution involved in the growth of a bubble, no other bubbles may nucleate as a consequence of the depleted gas concentration [22]. As the bubble keeps on growing, the subsequent step of bubble impingement has to be taken into account to consider bubble/bubble interactions. Typically, a few growing bubbles are considered and numerical models are used to investigate the evolution of the bubble wall thickness, state of stress and deformation [23–29]. Eventually, the bubble walls may rupture, due to the presence of structural inhomogeneities in the polymer matrix, either introduced from outside (e.g., solid particles) or generated inside the polymer (e.g., crystallization) [30–32]. In both cases, it is assumed that due to the presence of such inhomogeneities, a non-uniform deformation takes place, determining a high level of stress at the polymer-heterogeneity interface that, in turn, may lead to wall rupture.

The comprehensive picture of the state of the art of foaming modeling is reported in Fig. 1, as a scheme of the aforementioned sequence of operations, together with the most important scientific contributions that have dealt with the modeling of one or more of these operations.

Although the strategies for bubble wall rupture should lead, by definition, to open-cell foams, a close observation of the foam morphology, and, in particular, of the polymeric layer dividing two neighboring cells, usually shows that bubble walls are still present, even if broken (Fig. 2b). In this case, then, some of the properties may not conform to fully open-cell foams, in which the polymer is solely confined to the struts. Fig. 2 shows a clarifying example of a closed-cell foam (a), an open-cell foam with broken walls (b) and a fully open-cell foam, with no walls at all and with the polymer solely confined to cell struts (c).

In order to have a fully open-cell morphology, where no material occupies the bubble walls, it is not sufficient to produce a fracture within the wall, but a *bubble wall retraction* is needed. In metallic foams as well as in thermosetting polyurethane foams and soap bubbles, low viscosities and high surface energies are straightforward conditions for wall retraction, which can be very fast and easy [45,46]. In thermoplastic polymers, conversely, viscous forces can be much stronger than interfacial forces, hindering bubble wall retraction, thereby leading more easily to open-cell morphologies such as the one reported in Fig. 2b [31].

In this work, in order to achieve fully open-cell foams, we conduct a comprehensive analysis, by means of experimentally-validated modeling and numerical simulations, of the sequence of events leading to the formation of the foam and to the development and rupture of the bubble walls. In particular, we investigate in details the role of the polymer elastic recovery as an additional, crucial factor in the bubble wall retraction mechanism. Finally, the developed model allows the design of the material and the process to drive the foam to a fully open-cell morphology. Both the use of the elastic recovery as an additional (actually dominant, at least in thermoplastic polymers) retraction mechanism and the resulting design tool for final foam morphology control are the main novelties of the present contribution.

The approach was validated by using a homemade apparatus with a visualization window that was designed for microcellular foaming at different processing conditions (i.e. temperature and pressure). The thermoplastic polymer used during the experiments was a poly(ε-caprolactone) (PCL) foamed with CO_2. The experimental results were compared with the theoretical analysis, as it is shown in the result section.

2. Theoretical background and modeling

The present approach analyzes the foaming process, from bubble growth to bubble impingement and bubble wall opening, and is divided into four operations, as described in Fig. 3: single bubble growth (SBG), impingement (IM), bubbles wall rupture (RU), and bubbles wall retraction (RE). It is worth noticing, here, that we did not include the bubble nucleation stage in the model. The latter assumes that a given nuclei density is fixed and describes the growth, interaction and coalescence phenomena. In the following, we will describe in detail the different steps and their mutual interactions.

2.1. SBG

The single bubble growth (SBG) model describes the growth dynamics of an isolated bubble, driven by the presence of supersaturated gas within the polymeric matrix. Single bubble growth in a viscoelastic system is modeled through a detailed 3D mathematical description, by adapting a model, initially proposed by Everitt et al. [25], to the PCL/CO_2 case at hand. All relevant properties (rheological, sorption, volumetric and interfacial) have been either taken from the literature [11] or directly measured in the present work, as described below.

We consider a single spherical gas bubble with initial radius R_0 surrounded by a spherical shell of a viscoelastic liquid containing a given quantity of dissolved gas. The initial bubble volume is $V_0 = 4/3\pi R_0^3$ and the initial gas pressure in the bubble is p_{g0}. Bubble growth is driven by the difference between the actual gas pressure inside the bubble, p_g, and the external ambient pressure, p_a. We assume isothermal conditions, incompressibility of the viscoelastic fluid and negligible inertia.

Under the above conditions, the bubble growth dynamics are governed by the momentum balance equation for the liquid shell and by the diffusion equation of the gas from the liquid to the bubble. Because of the spherical symmetry of the system, we choose a spherical coordinate system with the origin coinciding with the bubble center. Furthermore, due to the liquid volume conservation, we transform the radial coordinate r into a Lagrangian volume coordinate x such that $r^3 = R^3 + x$ [24], where R is the time-dependent bubble radius. Therefore, $x = 0$ is the (Lagrangian) position of the bubble–liquid interface and $4/3\pi\, x$ is the liquid volume between a generic radial position inside the fluid shell and the

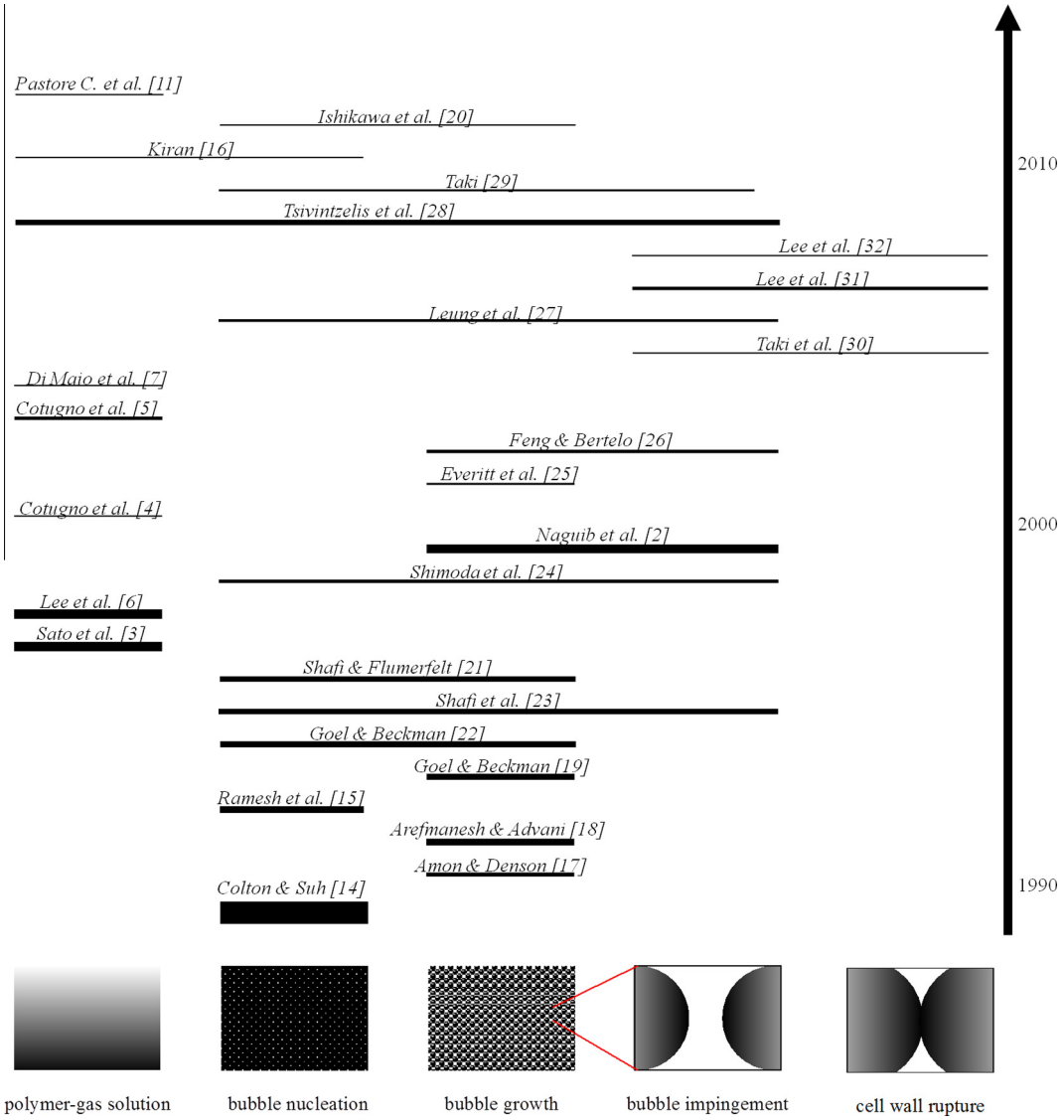

Fig. 1. Scheme of the sequence of operations leading to open-cell foams by gas foaming, together with the underlying literature that has dealt with the modeling of one or more of these operations. Lines below the references extend along the operations addressed to in the reference and line thickness is representative of its relative impact (as by the number of ISI citations as of June 2015).

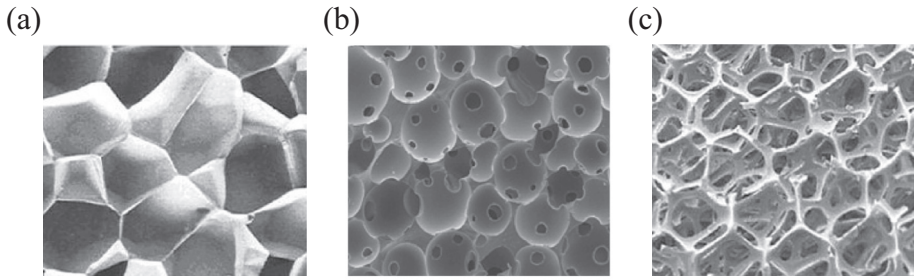

Fig. 2. Possible morphologies in thermoplastic foams: (a) closed cells, (b) open-cells with broken bubble walls, (c) fully open-cells with polymer confined to the struts.

bubble–liquid interface. We define $x = X$ the (Lagrangian) position of the outer edge of the liquid shell, thus $4/3\pi X$ is the volume of the whole shell. The boundary conditions are: (i) normal stresses at the outer liquid edge equal the ambient pressure; (ii) normal stresses at the bubble boundary equal the bubble pressure plus the surface tension contribution. In addition, we assume that Henry's law holds for the gas at the bubble–liquid interface. Finally, the Giesekus model [33] is chosen as the constitutive equation for the viscoelastic liquid, as it well describes the rheology of the neat PCL (see below).

We select the initial bubble radius, R_0, as length scale of the system, the ratio of the polymer viscosity, η_p, and the fluid relaxation time, λ, as stress scale, and the initial number of moles of the gas in the bubble $p_{g0}R_0^3/R_gT$, with R_g the universal gas constant and T the absolute temperature, as scale for the number of moles of the gas in the bubble.

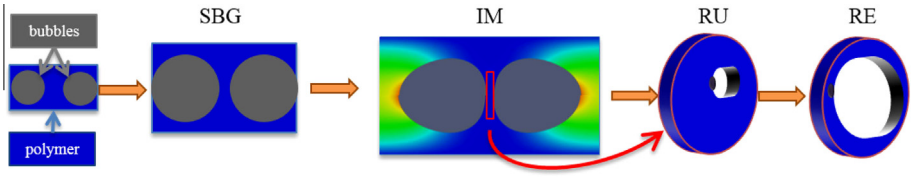

Fig. 3. Scheme of the foaming process to produce open-celled foams.

The following system of dimensionless equations results:

$$\frac{4}{3}\eta_r\frac{du}{dt}\left(\frac{1}{u}+\frac{1}{u+X}\right)=P_gWi+\frac{2}{3}\int_0^X\frac{T_{rr}-T_{\theta\theta}}{x+u}dx-\frac{1}{\Gamma u^{1/3}} \tag{1}$$

$$\begin{aligned}\frac{\partial T_{rr}}{\partial t}&=-\frac{4}{3(x+u)}\frac{du}{dt}T_{rr}-(T_{rr}-1)-\alpha(T_{rr}-1)^2\\ \frac{\partial(T_{rr}-T_{\theta\theta})}{\partial t}&=\frac{2}{3(x+u)}\frac{du}{dt}[(T_{rr}-T_{\theta\theta})-3T_{rr}]-(T_{rr}-T_{\theta\theta})\\ &\quad+\alpha(T_{rr}-T_{\theta\theta})(2-T_{rr}-T_{\theta\theta})\end{aligned} \tag{2}$$

$$\frac{\partial\phi}{\partial t}=N(x+u)^{4/3}\frac{\partial^2\phi}{\partial x^2} \tag{3}$$

$$\left(\frac{p_a+(p_{g0}-p_a)P_g}{p_{g0}}\right)u=1+\phi(0,t) \tag{4}$$

Eqs. (1)–(3) are the momentum balance for the liquid, the Giesekus constitutive equations, and the diffusion equation for the gas in the liquid, respectively. Eq. (4) derives from the mass conservation in the bubble. In these equations, $u(t)=R^3(t)$ is proportional to the bubble volume, $P_g=(p_g-p_a)/(p_{g0}-p_a)$, T_{rr} and $T_{\theta\theta}$ are the rr- and $\theta\theta$- components of the viscoelastic stress tensor, and ϕ is a concentration potential defined as $\partial\phi/\partial x=c-c_0$, where c and c_0 are the time dependent and initial gas molar concentrations in the liquid, respectively. The quantity ϕ is introduced for numerical reasons [18]. The parameter α is a constitutive parameter of the Giesekus equation that modulates the shear-thinning behavior (in the simulation $\alpha=0.03$). Furthermore, the following set of dimensionless parameters appears in Eqs. (1)–(4):

$$\begin{aligned}Wi&=\frac{(p_{g0}-p_a)\lambda}{\eta_p}\\ \Gamma&=\frac{u_0^{1/3}\eta_p}{2S\lambda}\\ N&=\frac{9D\lambda}{u_0^{2/3}}\\ \phi&=RTH\\ \eta_r&=\frac{\eta_s}{\eta_p}\end{aligned} \tag{5}$$

where the Weissenberg number, Wi, is the product of the rate of bubble growth and the liquid relaxation time, the capillary number, Γ, is the ratio of viscous forces and interfacial forces acting on the bubble, with S the surface tension and $u_0=R_0^3$, the timescale ratio, N, is the ratio of liquid relaxation time to gas diffusion time, with D the diffusivity, Φ is a dimensionless Henry's constant, and η_r is the ratio of solvent viscosity, η_s, to polymer viscosity, η_p, in the Giesekus model [33].

Eqs. (1)–(4) are supplied with initial and boundary conditions:

$$\begin{aligned}&u(0)=1\\ &T_{rr}(0)=T_{\theta\theta}(0)=1\\ &\phi(0)=0\end{aligned} \tag{6}$$

$$\begin{aligned}&\frac{\partial\phi}{\partial x}=\Phi\frac{p_{g0}-p_a}{p_{g0}}(P_g-1)\quad(x=0)\\ &\frac{\partial^2\phi}{\partial x^2}=0\quad(x=X)\end{aligned} \tag{7}$$

Eqs. (6) are the initial conditions for the bubble volume, the stress tensor and the mass concentration of the gas in the liquid layer. Eqs. (7) are the boundary conditions for the gas diffusion equation at the gas–liquid interface and at the outer liquid edge. Finally, the parameter X that accounts for the fluid volume surrounding the bubble also needs to be specified. Eqs. (1)–(4) with conditions (6) and (7) are numerically solved through the method of lines. The output of the SBG model is the single bubble growth kinetics, namely the evolution of bubble radius and gas pressure inside the bubble.

2.2. IM

The impingement (IM) model is intended to describe the relevant fluid dynamics when two (or more) bubbles come into contact.

In Fig. 4, a schematic view of two initially spherical bubbles with the same radius R_0 surrounded by the viscoelastic liquid is shown. An axis of symmetry, reported as a dash dot line in Fig. 4, can be identified, thus reducing the geometry to 2Ds. The liquid motion is governed by the mass and momentum balance equations given by:

$$\begin{aligned}&\nabla\cdot\boldsymbol{v}=0\\ &-\nabla p+\nabla\cdot\boldsymbol{T}=\boldsymbol{0}\end{aligned} \tag{8}$$

where $\boldsymbol{v}$, p and $\boldsymbol{T}$ are the fluid velocity, pressure and viscoelastic extra stress tensor fields, respectively. Axial symmetry is imposed on the boundary Γ_1, whereas symmetry is imposed on Γ_2 and Γ_4. In other words, the system consists of an infinite array of collinear, not necessarily equidistant, initially spherical bubbles that expand in a viscoelastic liquid. Outflow conditions are set on Γ_3.

On the gas–liquid interfaces $\Gamma_{b,1}$ and $\Gamma_{b,2}$, the Young–Laplace boundary condition holds:

$$\boldsymbol{T}\cdot\boldsymbol{n}=(-p_g+KS)\boldsymbol{n} \tag{9}$$

where $\boldsymbol{n}$ is the outwards normal to the bubble surface, and K is the surface curvature. The gas pressure p_g is related to the mass of gas inside the bubble, m_g, through the ideal gas law:

$$p_gV_g=m_gR_gT \tag{10}$$

with V_g the bubble volume.

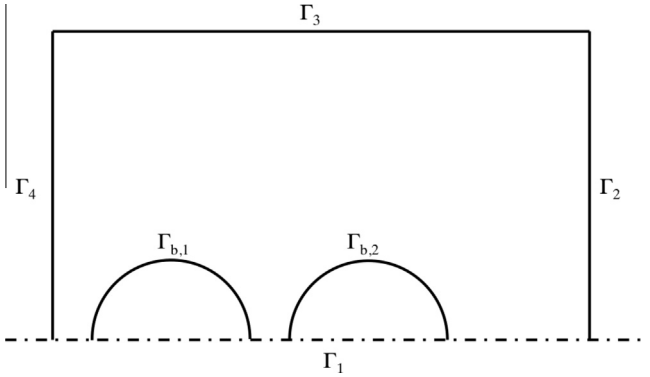

Fig. 4. Sketch of the geometry considered in the IM model.

The gas mass m_g can be computed from a mass balance at the gas–liquid interface, which in turn would require the solution of a diffusion equation in the liquid domain. To simplify the problem, we assume that the time evolution of the gas mass inside the bubble is given by the previously described SBG model under the same conditions (i.e., same liquid, physical properties, initial radius, pressures, etc.). Such an assumption is strictly valid as long as the bubbles grow as isolated spheres, namely at the short times. However, we do not expect significant qualitative changes even when the bubble shapes become distorted due to hydrodynamic interactions with their neighbors. This greatly simplifies the model as the diffusion equation is not required, the gas mass dynamics being known as an output from the SBG model.

Eq. (8) with boundary conditions (9) and (10) are solved through a finite element scheme. Outcomes of the IM model are the full stress and rate of strain tensor dynamics in the whole fluid domain, as well as the kinematics of the bubbles and, in particular, the time evolution of the liquid layer separating two bubbles.

2.3. RU

The rupture (RU) model is intended to describe the occurrence of rupture of the liquid layer separating two bubbles, therefore allowing to define specific rupture criteria. In the case of PCL, a semi-crystalline polymer, the occurrence of crystallization can be assumed as a rupture-inducing mechanism. Alternatively, rupture of the bubbles wall could be thought as triggered by the presence of solid additives.

It is known from the literature that polymer crystallization can be induced by flow. Such phenomenon, known as flow-induced crystallization (FIC), affects both processing and final sample properties [34]. The enhancement of the crystallization rate is attributed to a significant enhancement of the crystal nucleation rate, which is the first step in a crystallization process. Various models, both empirical and micro-rheological, can describe and predict the FIC process [35]. Elongational flow has been demonstrated to be more effective than shear flow in orienting the polymer chains and, therefore, enhancing the crystallization rate. Under this respect, we can define a Deborah number, $De = \lambda/t_f$, where $1/t_f$ is the inverse of the flow characteristic time, equal to either the shear rate, $\dot{\gamma}$, in shear flow or to the stretching rate, $\dot{\varepsilon}$, in extensional flow. The difference in the effects of elongational and shear flow on FIC increases with *De*, showing an appreciable deviation from $De = 0.3$ (see, for example, Fig. 3 in Coppola et al. [35]).

In foaming, the polymer occupying the space between the bubbles undergoes intense extensional flows, leading to an enhanced crystallization rate. In our case, the thin polymer layer between the gas bubbles is subjected to a position-dependent extensional flow field, reaching a maximum at the shortest distance between bubbles. There, the chances to crystallize are the highest possible, with the resulting crystal nuclei acting like heterogeneous particles, thus inducing rupture of the polymer layer. Based on these considerations, two possible rupture criteria can be defined: (i) in the case of FIC, rupture is assumed upon attainment of flow-enhanced crystallization conditions (i.e. $De = 0.3$); (ii) in the case of filled polymers, where rupture is induced by the presence of heterogeneities, the attainment of a liquid thickness between bubbles is equal to the significant size of the heterogeneity.

2.4. RE

As previously mentioned, the retraction of the thin film separating two bubbles is a necessary condition to achieve fully open-cell foams (see Fig. 2c). Retraction can only take place after rupture, when a "hole" is produced in the thin liquid film. Typically, retraction is imputed to the action of surface tension, which acts against the viscous forces in minimizing the interface area. In fact, the capillary number, Γ, regulates this retraction process. In some cases, such as soap bubbles, thermosetting flexible polyurethane foams or metal foams, surface forces are sufficiently larger than viscous forces [36] (i.e., $\Gamma \ll 1$). Bubble wall retraction is observed with the development of a fully open-cell structure, such as the one reported in Fig. 2c. In the case at hand, however, the PCL physical parameters under foaming processing conditions are such that surface tension induced retraction is not relevant. In fact, by using the following parameter values: $S = 2 * 10^{-2}$ N/m, $\eta_p = 10^5$ Pa * s, $\lambda = 0.15$ s and $R_0 = 10^{-5}$ m, one has $\Gamma \approx 10^2 \gg 1$, confirming that essentially no retraction is obtained by the action of interfacial tension. An alternative mechanism for retraction, therefore, must be considered. To this end, it is useful to remind that, depending on processing conditions, foaming can be a quite fast process, with complete expansion possibly achieved in a few seconds time. Consequently, the thinning of the liquid film separating bubbles can be very fast, too. Hence, by considering that we are dealing with a viscoelastic material, elastic recovery can be invoked as an additional mechanism for retraction, at least as long as the polymer relaxation time is longer than the foaming time. In this case, ruptured bubble walls may retract by the partial recovery of the strain in the extended polymer layer, driven by the elastic stress component.

A rough estimate of the fraction *X* of the area of the film separating two bubbles that can be recovered after the rupture event is given by $X = \dot{\varepsilon}_r \lambda$, where $\dot{\varepsilon}_r$ is the local stretching rate in the polymer at the rupture. To understand such an estimate, we may observe that the elastic elongational stress in the polymer film is "remembered" by the material for a time of the order of the polymer relaxation time. As a consequence, the relevant part of the recovered deformation is the one that has been built up along times shorter than λ. It is important to notice that the fraction of retracted area so defined corresponds to the Deborah number (i.e. *De*) at the rupture. This means that a retraction criterion can be defined on the basis of the *De* value reached at film rupture. The experimental availability of $\dot{\varepsilon}_r$ is not trivial, of course, since local measurements of film thickness and strain must be performed. In our case, however, the IM model yields the whole stress and strain tensor histories, thus $\dot{\varepsilon}_r$ can be easily evaluated.

The recovery-induced retraction, to the best of our knowledge, has not ever been applied to foaming, and in particular as a mechanism (and, hence, as a design tool) to drive closed- to open-cell morphologies. Despite the first observations of the retraction of thin liquid films were done on soap films long time ago [37,38], only recently film rupture has been used as a mean to measure the viscosity of molten polystyrene films [39,40]. Even more recently, the rupture of soap bubbles formed from a viscoelastic solution has been investigated with slow-motion imaging and experimental observations have been justified through a storing elastic energy that is released after the rupture, representing an additional driving force for film retraction [41]. In foaming, viscoelastic effects on foam morphology have not been considered yet. In the following, we thoughtfully describe our approach and how to derive information on foam morphology from growth dynamics. To clarify the interaction and flow of information among the modeled sequence of operations, Fig. 5 represents a flow-chart of the whole approach.

3. Materials and methods

3.1. Polymer and gas

PCL Capa™ 6800 with a melt flow index of 3.02 g/10 min, weight average molecular weight of 120 kDa and number average molecular weight of 69 kDa, has been supplied by Perstrop Holding

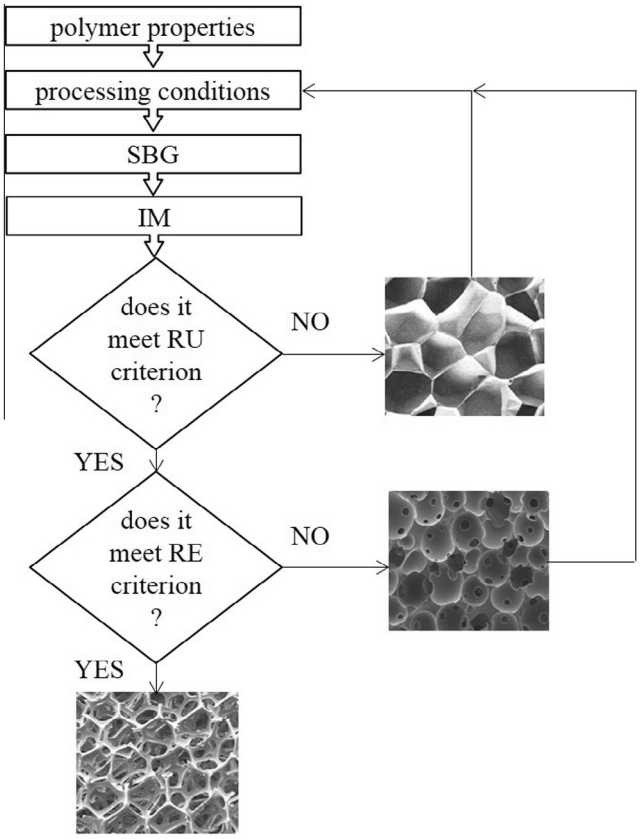

Fig. 5. Flow chart of the necessary operations for a fully open-celled structure.

AB, Sweden. Linear viscoelastic moduli of the polymer have been measured in the temperature range 60–130 °C under a nitrogen atmosphere using a strain-controlled Rheometric Scientific ARES rheometer (TA Instruments, USA) with parallel plates of 25 mm in diameter and a gap of about 1 mm. The strain amplitude has been set large enough to give a reliable signal while keeping the measurement in the linear viscoelastic regime (between 1% and 10%). Time sweep tests have been performed before the frequency sweep tests in order to measure the stability of the sample. A master curve has been constructed by using the horizontal shift factor with density compensation (Fig. 6b, the line is the Williams, Landel and Ferry fit). The viscoelastic response at 35 °C has been obtained by using the value of the corresponding (extracted) shift factor and it is reported in Fig. 6a. At 35 °C, the PCL shows a viscoelastic behavior with a relaxation time of about 0.2 s, calculated as the inverse of the cross over frequency in Fig. 6a.

To perform the foaming experiments, a PCL film has been obtained by hot compression molding at 90 °C and 10 MPa for 5 min. The thickness and the shape of the film have been controlled using a metal circular mold.

CO_2 (99.95% pure) supplied by Sol Group S.p.A., Italy, has been used as the physical blowing agent.

3.2. Foaming apparatus and visualization system

In order to validate the model two kinds of experiments were required. On the one hand, we performed foaming experiments at different processing conditions using a novel batch foaming apparatus, called mini-batch, to obtain information on the final foam morphology. 3D rendering images of the mini-batch are reported in Fig. 7. A complete description of the foaming batch is given in [42].

On the other hand, based on a previous apparatus for foam visualization [43,44], we designed a homemade pressurized vessel to allow the foaming visualization experiments. The pressurized vessel consists of a chamber with three transparent sapphire windows, a temperature port to control the temperature inside the vessel (as close as possible to the sample), a gas dosing/release port, and a pressure measurement port (see Fig. 8a). Two coaxial sapphire windows, placed at middle height of the vessel, are used to illuminate the chamber (light-cells), a third, smaller sapphire window, perpendicular to the other two windows, is used to visualize bubble formation in the PCL film (visualization cell). Fig. 8b shows an inside view of the chamber, where the PCL film is arranged on the bottom surface in front of the visualization cell.

3.3. Experimental procedure

Two series of experiments were performed by means of the mini-batch (i.e. for the validation of the final foam morphology) and foaming visualization (i.e. for the validation of the SBG) systems described in the previous section. Experiments were conducted by using the following procedure: PCL discs were saturated at 80 °C with CO_2 at different saturation pressures (P_{sat}) for four hours. The gas was injected into the chamber via a syringe pump. In each experiment, the PCL sample was placed between two perforated holders (as shown in Fig. 8c). A stainless steel sheet (2.5 mm in thickness) with a 2 mm hole punched out in the center was placed beneath the PCL sample, so that the latter was partially suspended in air; observation of foaming process was focused upon that region. After sample loading, the vessel was cooled to the foaming temperature T_{foam} = 35 °C with a controlled, repeatable cooling history. At the foaming temperature, the sample was pressure-quenched to ambient pressure, using a Pressure Drop Rate (*PDR*) of 100 MPa/s. All experiments were performed at the same saturation and foaming temperatures and *PDR*. At the end of gas-saturation step, therefore, P_{sat} and the gas mass fraction in the polymeric matrix, C_{sat}, are univocally correlated and can be indifferently used as a unique processing variable.

The foaming process was captured by a speed camera DMK 41AUO2 by Imaging Source, Germany, placed in front of the visualization-cell. The images were analyzed through ImageJ® in order to evaluate the growth of the bubble radius as a function of time.

4. Results and discussion

Firstly, the SBG model has been experimentally validated. The rapid pressure drop applied in the foaming visualization system causes a thermodynamic instability within the polymer/gas solution to initiate the foaming process. Fig. 9 shows four successive snapshots taken during the foaming process, as described in Section 3.3. The reader may observe numerous peripheral bubbles nucleated heterogeneously at the interface with the circular sample holders, and a single central bubble, which, by chance, has nucleated sufficiently far from the others. This occurrence allowed verifying the SBG model with experimental data. In Fig. 10, we report a comparison between the experimental data and the SBG model predictions in terms of the ratio between the actual and the initial bubble radius. It is worth remarking that the theoretical curve displayed in Fig. 10 is computed by solving Eqs. (1)–(4) with the values of the dimensionless parameters in Eq. (5) obtained from measured physical properties [11] and the operating conditions of the actual experimental system (i.e. those illustrated in Section 3.3). In Tables 1 and 2, the characteristic material parameters (extrapolated from Pastore Carbone et al. [11]) and the numerical values (as described in Section 2) are reported. It is clear that

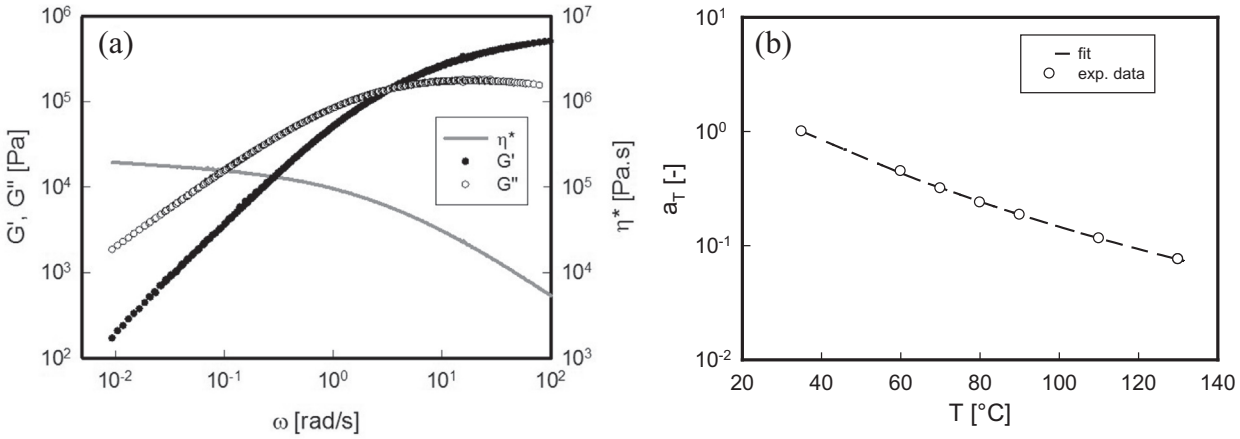

Fig. 6. (a) Superimposed linear viscoelastic moduli of PCL as a function of frequency at 35 °C; (b) horizontal shift factors as a function of temperature.

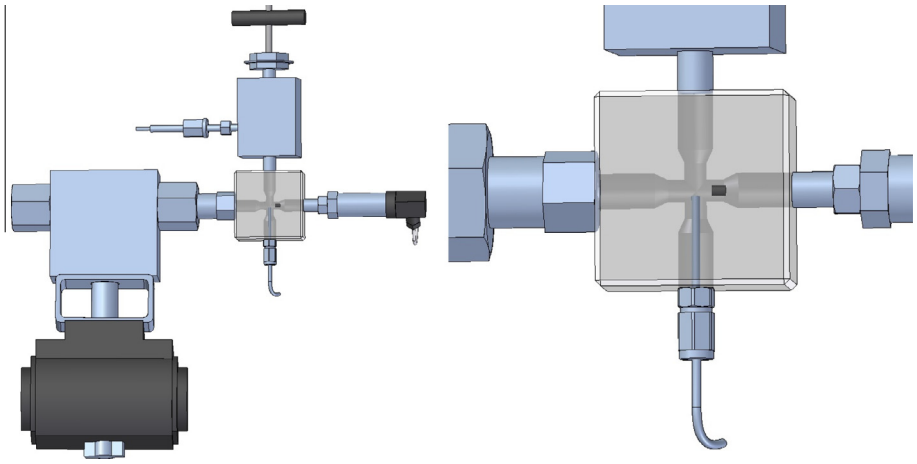

Fig. 7. 3D rendering of the mini-batch in two views and magnifications.

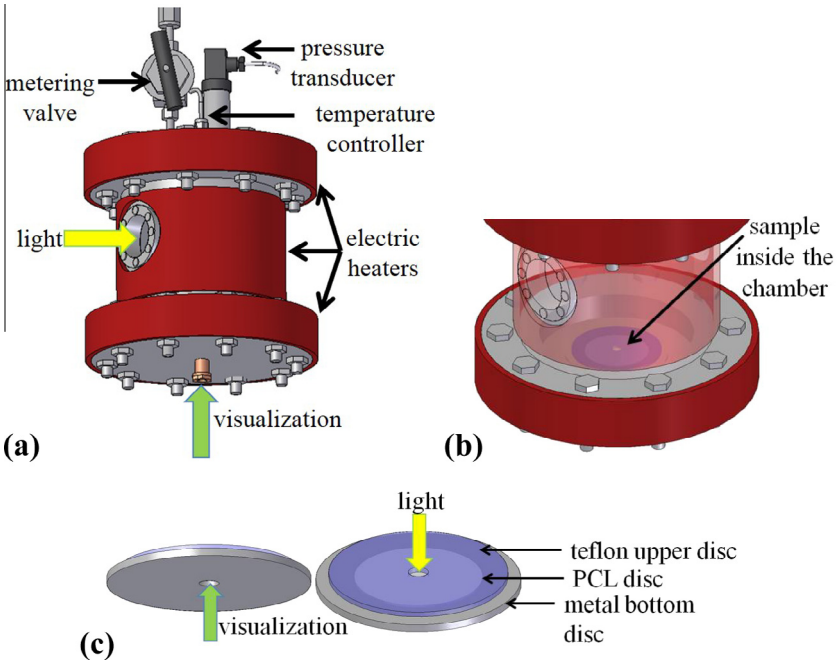

Fig. 8. (a) and (b) 3D rendering of foaming visualization batch, in two views and magnifications. (c) PCL sample between two sample-holders.

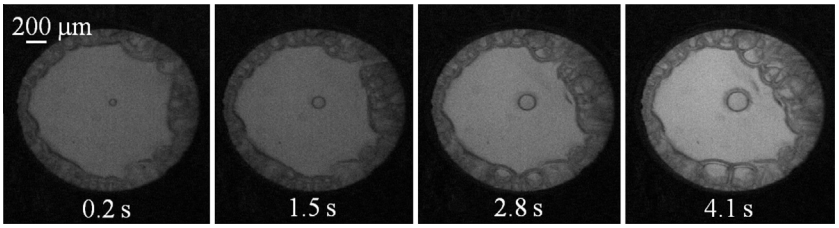

Fig. 9. Snapshots of PCL disc solubilized at P_{sat} = 5.8 MPa.

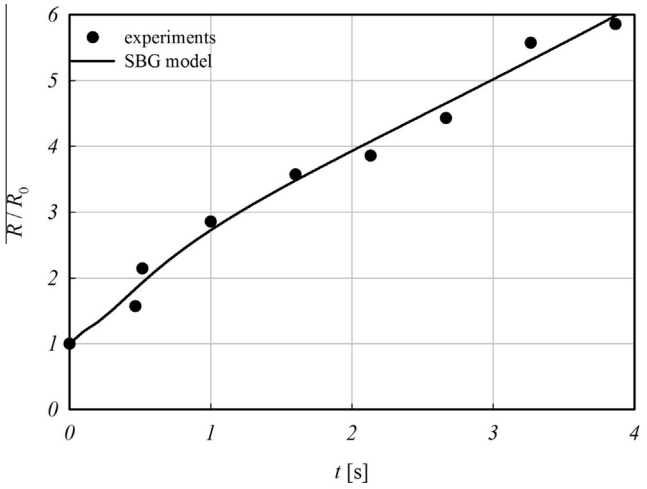

Fig. 10. Growth of a CO_2 bubble in PCL: comparison between experimental data (symbols) and SBG model predictions (line). The values of the parameters are reported in Table 1.

the SBG model predictions quantitatively agree with the experimental data in the first four seconds of the experiment.

The temporal evolution of the gas pressure $p_g(t)$ and bubble radius obtained from the SBG model is, then, used as an input for the IM step. Specifically, we studied the growth of a periodic array of initially equidistant bubbles of the same size. Through numerical simulations, we investigated the shape and stress evolution in the polymer layer surrounding the bubbles. In Fig. 11, the color maps of the first normal stress difference $N_1 = T_{rr} - T_{zz}$, with r and z the radial and axial coordinates of a cylindrical reference frame centered on the line connecting the centers of the bubbles, are shown at four consecutive times. Due to the axial symmetry of the problem, in Fig. 11 a section of the 3D geometry on an rz-plane is displayed, the azimuthal coordinate being irrelevant. The parameters used in the simulation shown in Fig. 11 are the same of the SBG simulation (Table 1). The initial radius of the bubble is R_0 = 10 μm, the initial thickness of the layer between the bubbles is δ_0 = 37.5 μm (δ is defined in Fig. 11). This value has been determined from SEM micrographs of the final foam morphology, by measuring the average distance among the centers of the cells and the final foam density. This is a key point in the current modeling approach and allows not to include the bubble nucleation phenomenon. As expected, when the two bubbles start to interact

Table 1
Numerical values of the physical parameters used in the model for the system PCL/CO_2, considering the processing conditions (i.e. 35 °C and 5.8 MPa).

Henry constant (H) [mol/(N * m)]	Interfacial tension (S) [mN/m]	Diffusivity (D) [m^2/s]	Specific volume ($1/\rho$) [m^3/kg]
$5.2 * 10^{-5}$	19.3	$3.5 * 10^{-10}$	918.1

Table 2
Numerical values of the dimensionless parameters used in the numerical solution of the SBG model.

Wi	1.167
Γ	3158
N	0.0468
Φ	1.288
η_r	0
X	729

(see t = 1 s in Fig. 11) the maximum N_1-value is located at the middle of the line connecting the centers of the bubbles (in the point A, i.e. $N_{1,A}$). As the bubbles grow, such value increases as a consequence of the increasing stretching rate in the inter-bubble layer.

The simulation results provide the temporal evolution of all quantities of interest. In particular, the thickness δ of the layer between the bubbles, plotted in Fig. 12, monotonically decreases in time from its initial value δ_0 as bubbles are approaching.

It is worth noting that the slope of δ as function of time changes passing through an inflection point between 1.5 and 2 s (see Fig. 12). This is due to the predicted strain hardening of the fluid subjected to high stretching rates, which is an important phenomenon in the bubble coalescence process, as already reported elsewhere [48]. Due to the flow induced higher viscosity of the polymer medium between the two approaching bubbles, the thinning kinetics of the layer, consequently, slow down.

On the basis of the results provided by SBG and IM steps, we are now in a position to evaluate the rupture of the polymer layer and its possible retraction. In this regard, we recall that it is known from the literature that, for crystallizing polymers, the crystallization event occurs when De locally reaches values of about 0.3 [35]; such an event can be responsible for rupture of the polymer layer. In case the stresses in the liquid around the rupture point are sufficiently large, retraction of the polymer layer can happen.

In order to study the different morphologies that can be obtained in PCL foams, we performed two sets of experiments at different saturation pressures: $P_{sat,1}$ = 5.5 MPa and $P_{sat,2}$ = 10 MPa. All other processing parameters have been kept constant, i.e., temperature T = 35 °C and PDR = 10 MPa/s. The SEM images in Fig. 13 confirm that different morphologies are indeed obtained. For the lower P_{sat} (Fig. 13a), a closed-cell morphology is obtained, where the gas cells are clearly separated by polymer layers. Conversely, at the higher saturation pressure (Fig. 13b), the cells are not clearly distinguishable.

We run numerical simulations of the SBG and IM of two systems characterized by the same processing conditions as the experiments discussed above. Specifically, for the system in Fig. 13a, the initial thickness of the polymer film is δ_0 = 60 μm, whereas, for the system in Fig. 13b, it is δ_0 = 37.5 μm; in both cases, the initial radius of the bubbles is R_0 = 10 μm. In Fig. 14, we report, for the two cases, the time evolution of the maximum De, that is, the one evaluated at point A (De_A). As no additive is present in the polymer and since PCL is a crystallizing polymer, we expect

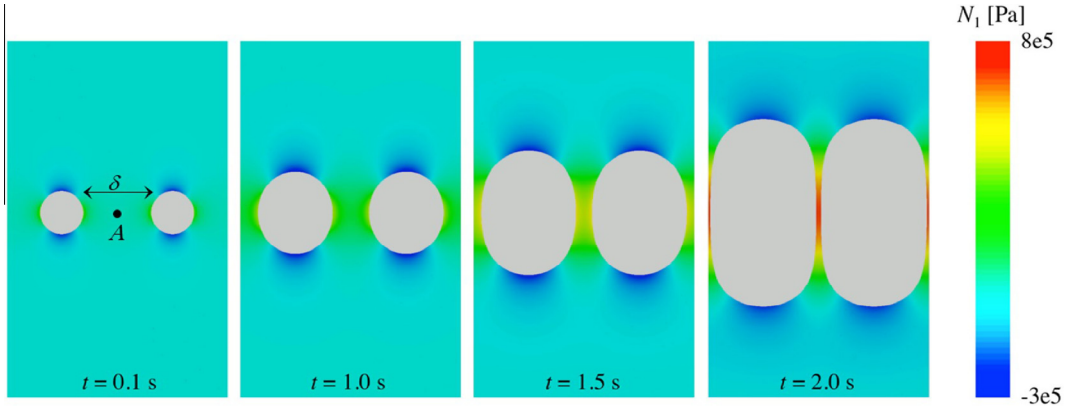

Fig. 11. Color maps of the first normal stress difference N_1 in the polymer surrounding two bubbles at increasing times for R_0 = 10 μm, δ_0 = 37.5 μm and the values of the parameters in Table 1. *A* is the middle point of the line connecting the centers of two bubbles. (For interpretation of the references to colour in this figure legend, the reader is referred to the web version of this article.)

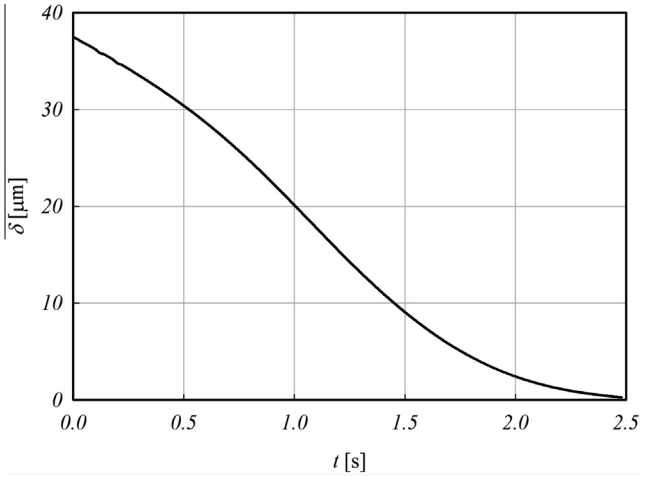

Fig. 12. Time evolution of the thickness δ of the polymer layer between two equidistant bubbles for R_0 = 10 μm, δ_0 = 37.5 μm and the values of the parameters in Table 1.

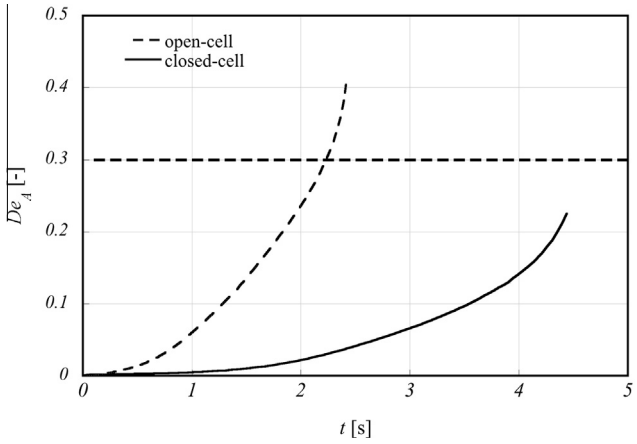

Fig. 14. Temporal evolution of De_A computed at the middle point of the line connecting centers of two approaching bubbles for $P_{sat,1}$ = 5.5 MPa (solid curve) and $P_{sat,2}$ = 10 MPa (dashed curve).

that rupture is caused by *FIC*. It is worth of note that, even if it is impossible to quantitatively indicate the quiescent induction time for PCL in the same operative conditions, we can speculate that the *FIC* time would be surely faster than the quiescent one [47]. The simulations end when the thickness of the film between the bubbles goes to zero. In the first case, characterized by P_{sat} = 5.5 MPa, De_A does not reach the threshold value of 0.3 necessary for crystallization (red curve). Hence, in agreement with the experiments, a closed-cell structure is predicted. On the contrary, for P_{sat} = 10 MPa, the De_A overcomes the threshold value at about *t* = 2.2 s (green curve). Crystallization-induced rupture can take place, thus yielding an open-cell structure compatible with the experimental one shown in Fig. 13b.

The procedure so far developed can be used to design materials and processing conditions to obtain desired morphologies for a pure, semi-crystalline polymeric material. In particular, the rate of bubble inflation, strictly related to the initial overpressure but also to all the material physical properties, can be used as a tool to control the morphology. In fact, when conditions are such that

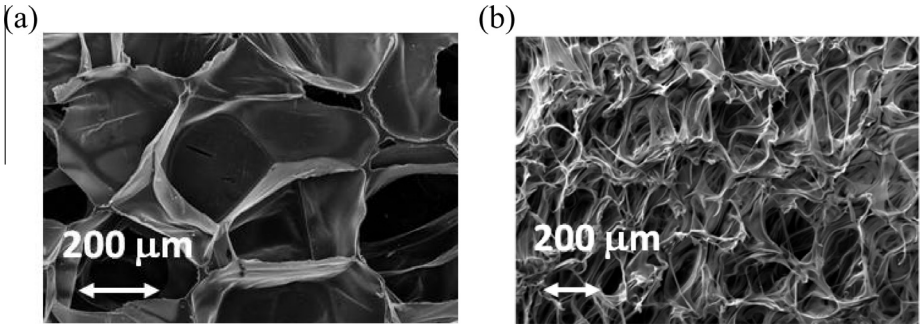

Fig. 13. SEM images of PCL foams. (a) closed-cell morphology (b) fully open-cell morphology.

flow-induced crystallization takes place within the stretched bubble wall layer, rupture is expected to set in. The same basic principles can be used, however, also in the case of filled polymeric materials. Let us consider, for example, an amorphous polymer, where crystallization-induced rupture cannot take place. As previously remarked, however, the solid particle in-homogeneities embedded in the matrix can induce rupture in a very similar way when the wall bubble thickness becomes comparable to the significant particle size. In this case, obviously, the properties of the expanding polymer, which are responsible for its foaming behavior, can be severely affected by the presence of the additive. For instance, additives may work as nucleating agents for the bubbles, thereby modifying the foam morphology, as well as the rheological and surface properties. Of course, it is possible to measure those properties and, as it has been done throughout this work, adapt the starting conditions of the model (e.g. R_0 and δ_0) to the observed morphology.

In spite of the above-mentioned complication, the very final stages of bubble rupture and possible retraction are expected to be always dictated by the local interactions between the stress/strain evolution and the wall geometrical parameters. To make this point clear we may suppose, in a simplistic manner, that properties and morphologies do not change and, with reference to the foaming conditions reported in Table 1, the same bubbles dynamics and interaction holds, also in case where solid particles are embedded in the polymer. Fig. 15 shows the temporal evolution of δ, the first normal stress difference at point A $N_{1,A}$, and De_A. When a particle of

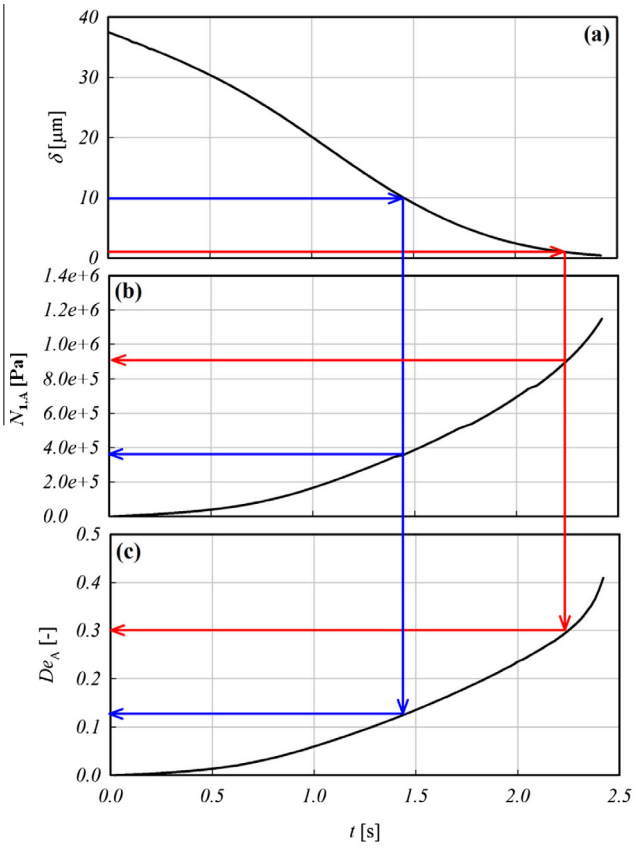

Fig. 15. Time evolution of the thickness of the layer between two consecutive bubbles δ (a), of the first normal stress difference $N_{1,A}$ (b), and of De_A (c) from numerical simulations. The operating parameters are reported in Table 1, the initial radius of the bubbles is R_0 = 10 μm and the initial thickness of the polymer layer is δ_0 = 37.5 μm. The lines are guides for the eye, indicating the addition of 10 μm solid particles (blue line) and 1 μm solid particles (red line). (For interpretation of the references to colour in this figure legend, the reader is referred to the web version of this article.)

10 μm characteristic size is used, we expect that the polymeric film breaks when its thickness reaches approximately the same size. As shown in Fig. 15 (blue line), this happens at t = 1.4 s. Here, the first normal stress difference is $N_{1,A} \approx 4 * 10^5$ Pa and the $De_A \approx 0.14$. Under such conditions, a certain, limited, amount of retraction will take place as predicted by the described retraction criterion (see Section 2 section RE). In case the solid particle is 1 μm in size, the polymeric film is expected to break after about 2.25 s (vertical red line in Fig. 15). Here, $N_{1,A}$ is about $9 * 10^5$ Pa and De_A is about 0.3. In this latter case, due to the higher elastic energy stored in the polymer layer at rupture, a much more pronounced retraction is expected with respect to the previous case, likely leading to a morphology similar to the one shown in Fig. 13b. As a partial conclusion of this speculation on the size of the additives, while it could be erroneously thought that breaking the bubbles wall earlier (by using bigger particles) could be beneficial for achieving an open-cell morphology, we prove, conversely, that it is necessary to use smaller particles to retard the bubbles wall rupture, to allow the build-up of stresses in order to increase the elastic recovery of the bubbles wall and, in turn, to have a fully open-cell foam. It is worth to stress here that for the sake of simplicity we implicitly assumed spherical and monodispersed particles, while foaming nucleating additives are often very far from being spherical (e.g. platelets or aciculae). The inclusion of anisotropic particles in the model (both the IM and RU, but also the SBG and RE, to a lesser extent) would obviously add difficulties to the present approach. More specifically, we can speculate that the significant size for the cell opening could change during the foaming process, according to the tumbling process of the anisotropic particles. We consider this, however, out of the scope of the present contribution, and will be a matter of future work.

5. Conclusions

In this paper, we develop a novel approach to cell-opening in thermoplastic foams. The procedure is based on sequential steps. Single bubble growth modeling results are used as an input for the impingement model where two bubbles surrounded by a viscoelastic fluid grow and hydrodynamically interact. We identify a criterion that employs the computed stresses, the elongational rate and the film thickness to predict the rupture of the polymeric layer between the bubbles and its retraction. As a result, the model is able to make predictions on the final foam morphology, starting from the gas polymer solution properties. We performed independent experiments to assess the validity of each step of our approach. In conclusion, the developed methodology allows to design the materials and processing conditions to control foam morphology.

As a concluding remark, it is worth of note that the current work brings three independent contributions:

- A numerical simulation approach that covers the foaming process from bubble growth to cell wall rupture and retraction was developed for a viscoelastic liquid. The result is a time evolution of bubbles and of the bubbles wall during the foaming process.
- The rupture and retraction criteria, tied at the time evolution of bubbles, were proposed to predict the final foam morphology (i.e. closed cells, open cells with broken bubble walls or fully open cells with polymer confined to the struts). The retraction criterion, introduced in the present contribution, represents a novel brick in the fundamental understanding of cell opening in thermoplastic foaming.
- The present approach allows designing the foaming process and the additives for the specific aimed morphology.

Acknowledgements

Rete di Eccellenze Mastri (MAteriali e STRutture Intelligenti, POR Campania FSE 2007/2013, Codice 4-17-3) and Procter and Gamble Company (Newcastle Innovation Centre, Whitley Road, Longbenton, NE12 9TS, United Kingdom) are acknowledged for partial support of this work.

References

[1] S.T. Lee, C.B. Park, Foam Extrusion: Principles and Practice, CRC Press, 2014.
[2] H.E. Naguib, C.B. Park, U. Panzer, N. Reichelt, Strategies for achieving ultra-low-density polypropylene foams, Polym. Eng. Sci. 42 (2002) 1481–1496.
[3] Y. Sato, T. Takikawa, A. Sorakubo, S. Takishima, H. Masuoka, M. Imaizumi, Solubility and diffusion of carbon dioxide in biodegradable polymers, Ind. Chem. Eng. Res. 16 (1) (2000) 1029–1034.
[4] S. Cotugno, E. Di Maio, C. Ciardiello, S. Iannace, G. Mensitieri, L. Nicolais, Sorption thermodynamics and mutual diffusivity of carbon dioxide in molten polycaprolactone, Ind. Chem. Eng. Res. 42 (19) (2003) 4398–4405.
[5] S. Cotugno, E. Di Maio, G. Mensitieri, S. Iannace, G.W. Roberts, R.G. Carbonell, H. B. Hopfenberg, Characterization of microcellular biodegradable polymeric foams produced from supercritical carbon dioxide solutions, Ind. Chem. Eng. Res. 44 (2005) 1795–1803.
[6] M. Lee, C.B. Park, C. Tzoganakis, Measurements and modeling of PS/supercritical CO, solution viscosities, Polym. Eng. Sci. 39 (1999) 99–109.
[7] E. Di Maio, S. Iannace, G. Mensitieri, L. Nicolais, Predictive approach based on the simha–somcynsky free-volume theory for the effect of dissolved gas on viscosity and glass transition temperature of polymeric mixtures, J. Polym. Sci. 43 (2006) 56–89.
[8] C.D. Han, C.Y. Ma, Rheological properties of mixtures of molten polymer and fluorocarbon blowing agent. I. Mixtures of low-density polyethylene and fluorocarbon blowing agent, J. Appl. Polym. Sci. 56 (1983) 28–851.
[9] L.J. Gerhardt, C.W. Manke, E.J. Gulari, Rheology of polydimethylsiloxane swollen with supercritical carbon dioxide, J. Polym. Sci. 35 (1997) 69–523.
[10] J.R. Royer, Y.J. Gay, M. Adams, J.M. De Simone, S.A. Khan, Polymer melt rheology with high-pressure CO_2 using a novel magnetically levitated sphere rheometer, J. Polym. 43 (2002) 2356–2375.
[11] M.G. Pastore Carbone, E. Di Maio, G. Scherillo, G. Mensitieri, S. Iannace, Solubility, mutual diffusivity, specific volume and interfacial tension of molten PCL/CO_2 solutions by a fully experimental procedure: effect of pressure and temperature, J. Supercrit. Fluids 30 (2012) 303–309.
[12] S.G. Kazarian, K.L. Andrew Chan, V. Maquet, A.R. Boccaccini, Characterisation of bioactive and resorbable polylactide/Bioglass® composites by FTIR spectroscopic imaging, Biomaterials 25 (2004) 3931–3938.
[13] M.G. Pastore Carbone, E. Di Maio, P. Musto, A. Braeuer, G. Mensitieri, On the unexpected non-monotonic profile of specific volume observed in PCL/CO_2 solutions, Polymer 56 (2015) 252–289.
[14] J.S. Colton, N.P. Suh, Nucleation of microcellular thermoplastic foam with additives: part I: theoretical considerations, Polym. Eng. Sci. 27 (1987) 485–492.
[15] N.S. Ramesh, D.H. Rasmussen, G.A. Campbell, The heterogeneous nucleation of microcellular foams assisted by the survival of microvoids in polymers containing low glass transition particles. Part I: mathematical modeling and numerical simulation, Polym. Eng. Sci. 34 (1994) 452–478.
[16] E. Kiran, Foaming strategies for bioabsorbable polymers in supercritical fluid mixtures. Part I. Miscibility and foaming of poly(l-lactic acid) in carbon dioxide + acetone binary fluid mixtures, J. Supercrit. Fluids 54 (2010) 296–307.
[17] M. Amon, C.D. Denson, Study of the dynamics of foam growth: simplified analysis and experimental results for bulk density in structural foam molding, Polym. Eng. Sci. 26 (1986) 255–267.
[18] A. Arefmanesh, S.G. Advani, Diffusion-induced growth of a gas bubble in a viscoelastic fluid, Rheol. Acta 283 (1991) 274–283.
[19] S.K. Goel, E.J. Beckman, Generation of microcellular polymeric foams using supercritical carbon dioxide. I: effect of pressure and temperature on nucleation, Polym. Eng. Sci. 34 (1994) 1137–1147.
[20] T. Ishikawa, K. Taki, M. Ohshima, Visual observation and numerical studies of N_2 vs CO_2 foaming behavior in core-back foam injection molding, Polym. Eng. Sci. 56 (2012) 659–691.
[21] M.A. Shafi, R.W. Flumerfelt, Initial bubble growth in polymer foam processes, Chem. Eng. Sci. 52 (1997) 627–633.
[22] S.K. Goel, E.J. Beckman, Nucleation and growth in microcellular materials: supercritical CO_2 as foaming agent, AIChE J. 41 (1995) 357–367.
[23] M.A. Shafi, J.G. Lee, R.W. Flumerfelt, Prediction of cellular structure in free expansion polymer foam processing, Polym. Eng. Sci. 36 (1996) 1950–1959.
[24] M. Shimoda, I. Tsujimura, M. Tanigaki, M. Ohshima, Polymeric foaming simulation for extrusion processes, J. Cell. Plast. 37 (2001) 517–536.
[25] S.L. Everitt, O.G. Harlen, H.J. Wilson, Bubble growth in a two-dimensional viscoelastic foam, J. Non-Newton Fluid Mech. 137 (2006) 46–59.
[26] J.J. Feng, C.A. Bertelo, Prediction of bubble growth and size distribution in polymer foaming based on a new heterogeneous nucleation model, J. Rheol. 48 (2004) 439.
[27] S.N. Leung, C.B. Park, D. Xu, H. Li, R.G. Fenton, Computer simulation of bubble-growth phenomena in foaming, Ind. Eng. Chem. Res. 45 (2006) 7823–7831.
[28] I. Tsivintzelis, A.G. Angelopoulou, C. Panayiotou, Foaming of polymers with supercritical CO_2: an experimental and theoretical study, Polymer 48 (2007) 5928–5939.
[29] K. Taki, Experimental and numerical studies on the effects of pressure release rate on number density of bubbles and bubble growth in a polymeric foaming process, Chem. Eng. Sci. 63 (2008) 3643–3653.
[30] K. Taki, K. Tabata, S. Kihara, M. Ohshima, Bubble coalescence in foaming process of polymers, Polym. Eng. Sci. 51 (2006) 1241–1259.
[31] P.C. Lee, J. Wang, C.B. Park, Extruded open-cell foams using two semicrystalline polymers with different crystallization temperatures, Ind. Eng. Chem. Res. 45 (2006) 175–181.
[32] P.C. Lee, G. Li, J.W.S. Lee, C.B. Park, Improvement of cell opening by maintaining a high temperature difference in the surface and core of a foam extrudate, J. Cell. Plast. 43 (2007) 431–444.
[33] R.W. Kolkka, G.R. Ierley, Phase space analysis of the spurt phenomenon for the Giesekus viscoelastic fluid model, J Non-Newton Fluid Mech. 33 (1989) 305–323.
[34] R.L. Miller, Flow Induced Crystallization in Polymer Systems, Gordon and Breach, London, 1979.
[35] S. Coppola, N. Grizzuti, P.L. Maffettone, Microrheological modeling of flow induced crystallization, Macromolecules 34 (2001) 5030–5036.
[36] S. Hartland, Surface and Interfacial Tension: Measurement, Theory, and Application, Marcel Denkker Inc., 2006.
[37] M.A. Dupré, Sixiéme memoire sur la theorie méchanique de la chaleur, Ann. Chim. Phys. 4 (1967) 194–220.
[38] Lord. Rayleigh, Some applications of photography, Nature 44 (1891) 249–254.
[39] K. Dalnoki-Veress, B.G. Nickel, C. Roth, J.R. Dutcher, Hole formation and growth in freely standing polystyrene films, J. Fluid Mech. 59 (1999) 2153–2156.
[40] C.B. Roth, B. Deh, B.G. Nickel, J.R. Dutcher, Evidence of convective constraint release during hole growth in freely standing polystyrene films at low temperatures, Phys. Rev. 72 (2005) 021802.
[41] E. Sabadini, R.F.S. Ungarato, P.B. Miranda, The elasticity of soap bubbles containing wormlike micelles, Langmuir 30 (2014) 727–732.
[42] D. Tammaro, V. Contaldi, M.G. Pastore Carbone, E. Di Maio, S. Iannace, A novel lab-scale batch foaming equipment: the mini-batch, J. Cell. Plast. 2 (2015) 654.
[43] Q. Guo, J. Wang, C.B. Park, M. Ohshima, A microcellular foaming simulation system with a high pressure-drop rate, Ind. Eng. Chem. Res. 45 (2006) 6153–6161.
[44] A. Wong, R.K.M. Chu, S.N. Leung, C.B. Park, J.H. Zong, A batch foaming visualization system with extensional stress-inducing ability, Chem. Eng. Sci. 66 (2011) 55–63.
[45] J. Banhart, Metal foams: production and stability, Adv. Eng. Mater. 8 (2006) 781–794.
[46] G. Harikrishnan, T.U. Patro, D.V. Khakhar, Polyurethane foam clay nanocomposites: nanoclays as cell openers, Ind. Eng. Chem. Res. 45 (2006) 7126–7134.
[47] S. Acierno, E. Di Maio, S. Iannace, N. Grizzuti, Structure development during crystallization of polycaprolactone, Rheol. Acta 45 (2006) 387–392.
[48] Y. Otsuki, T. Kanai, Numerical simulation of bubble growth in viscoelastic fluid with diffusion of dissolved foaming agent, Polym. Eng. Sci. 45 (2005) 1277–1287.